Supporting Information:

Carbon Dots Enhanced Graphene Field Effect Transistors for Ultrasensitive Detection of Exosomes

Sami Ramadan,[#,] Richard Lobo,† Yuanzhou Zhang,[#] Lizhou Xu,[# *] Olena Shaforost,[#] Deana Kwong Hong Tsang,[#] Jingyu Feng,† Tianyi Yin,[#] Mo Qiao,† Anvesh Rajeshirke,[#] Long R Jiao,†† Peter K.Petrov,[#] Iain E.Dunlop,[#] Maria-Magdalena Titirici,† and Norbert Klein[#]*

[#] Department of Materials, Imperial College London, London, SW7 2AZ, UK.

†Department of Chemical Engineering, Imperial College London, South Kensington Campus, London SW7 2AZ, U.K.

††Department of Hepatobiliary Surgery, Division of Surgery & Cancer, Imperial College London, Hammersmith Hospital Campus, Du Cane Road, London, W12 0NN, UK.

*Corresponding Authors: Dr. Sami Ramadan (s.ramadan@imperial.ac.uk); Dr. Lizhou Xu (l.xu@imperial.ac.uk)

Section S1. Characterization of carbon dots (CDs)

- **Photoluminescence measurements**

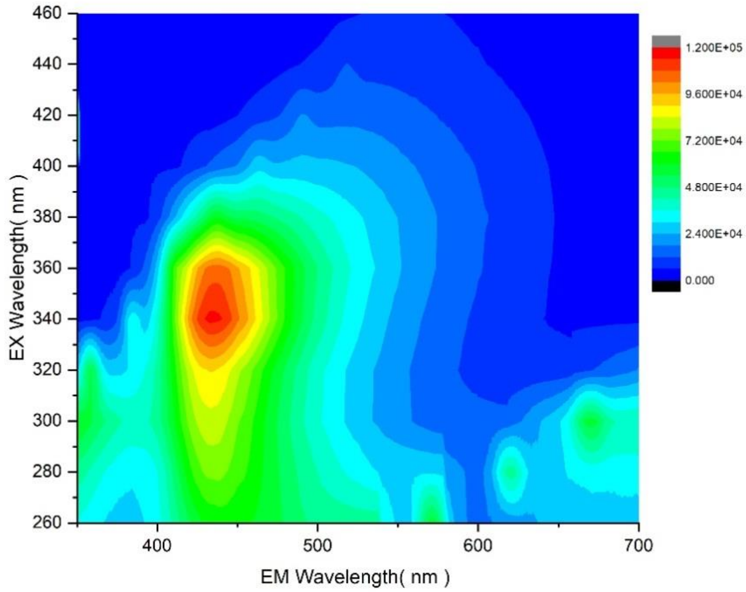

Figure S1. PL measurements of CDs. The CDs used in this study show blue-green emission predominantly and are most emissive when excited in the UV range (in this case between 320 – 360nm), with excitation-dependent emission at higher wavelengths.

Section S2. XPS and Raman characterization of surface functionalization process

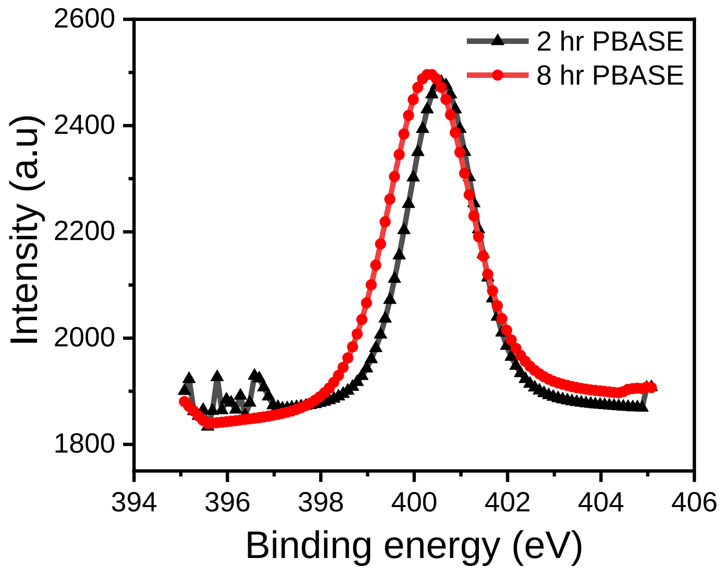

Figure S2. N1 s XPS spectra of graphene with 2 different PBASE exposure durations (Measurements were performed under the same conditions).

Table S1. N1s peak properties for different PBASE treatment times

PBASE exposure time (hr)	Average peak position (eV)	FWHM (eV)	Average normalized area
2	400.32	2.11	14.10
8	400.56	1.76	12.31

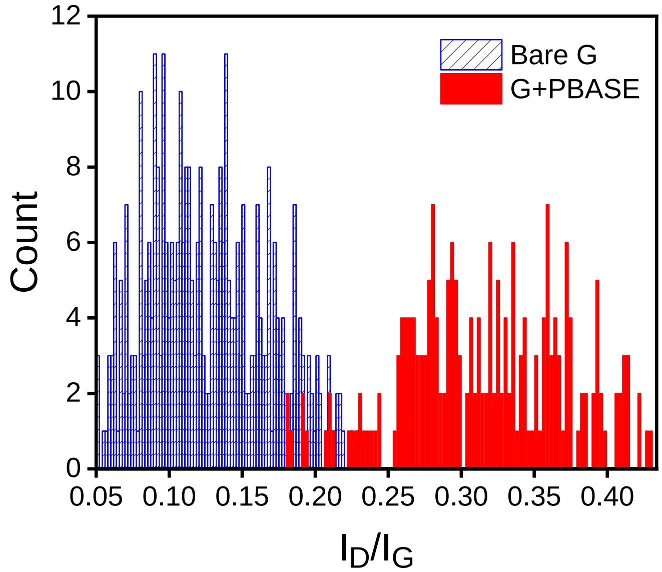

Figure S3. Histogram of I_D/I_G of as-transferred graphene and after PBASE functionalization of graphene surface.

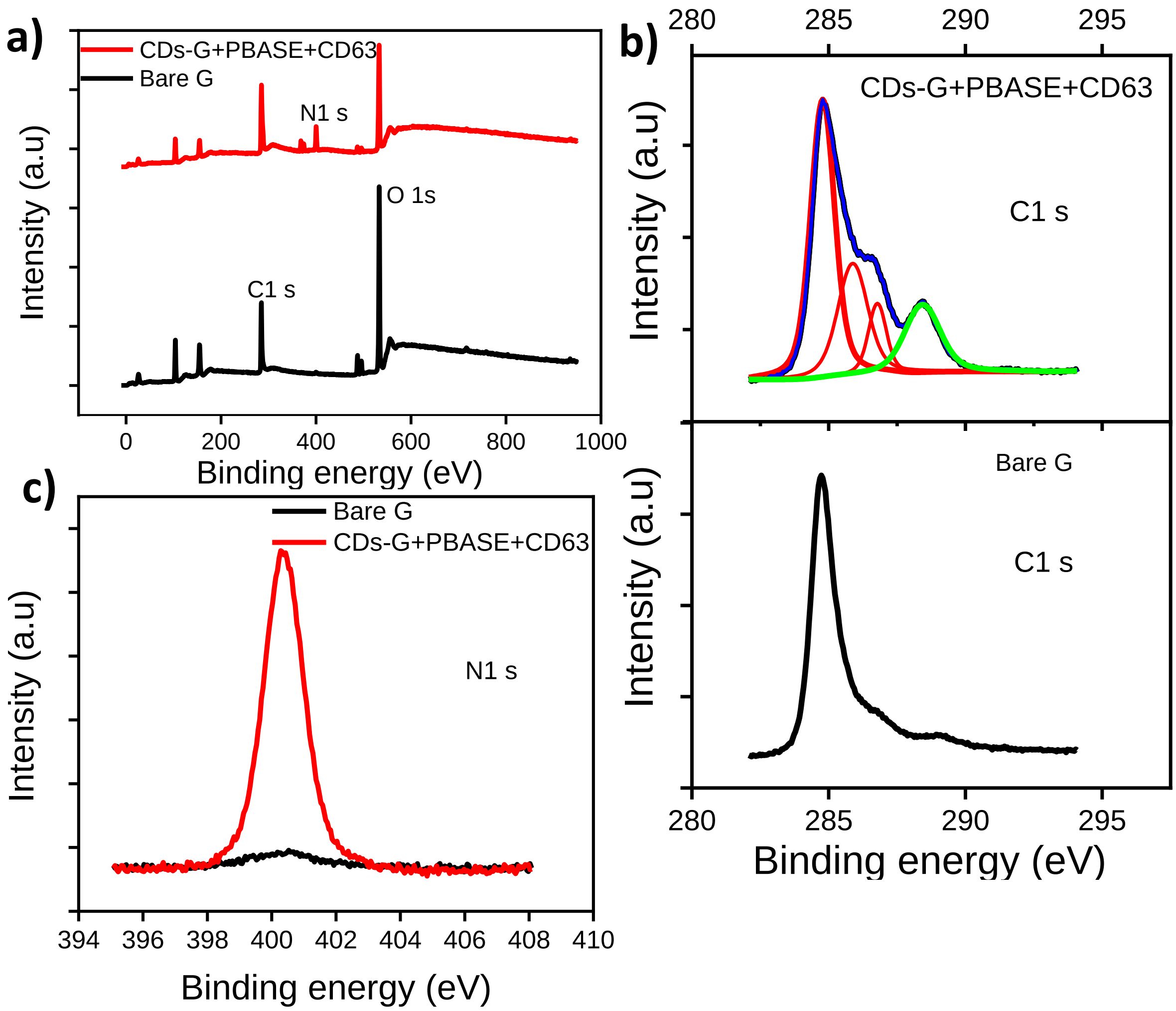

Figure S4. XPS survey spectra of the bare graphene and CDs functionalized with PBASE and antibody; C1 s and (j) N1 s XPS spectra of graphene with different levels of functionalization: bare, CDs-G with PBASE + anti-CD63 antibody.

Section S3. Exosome and antibody test

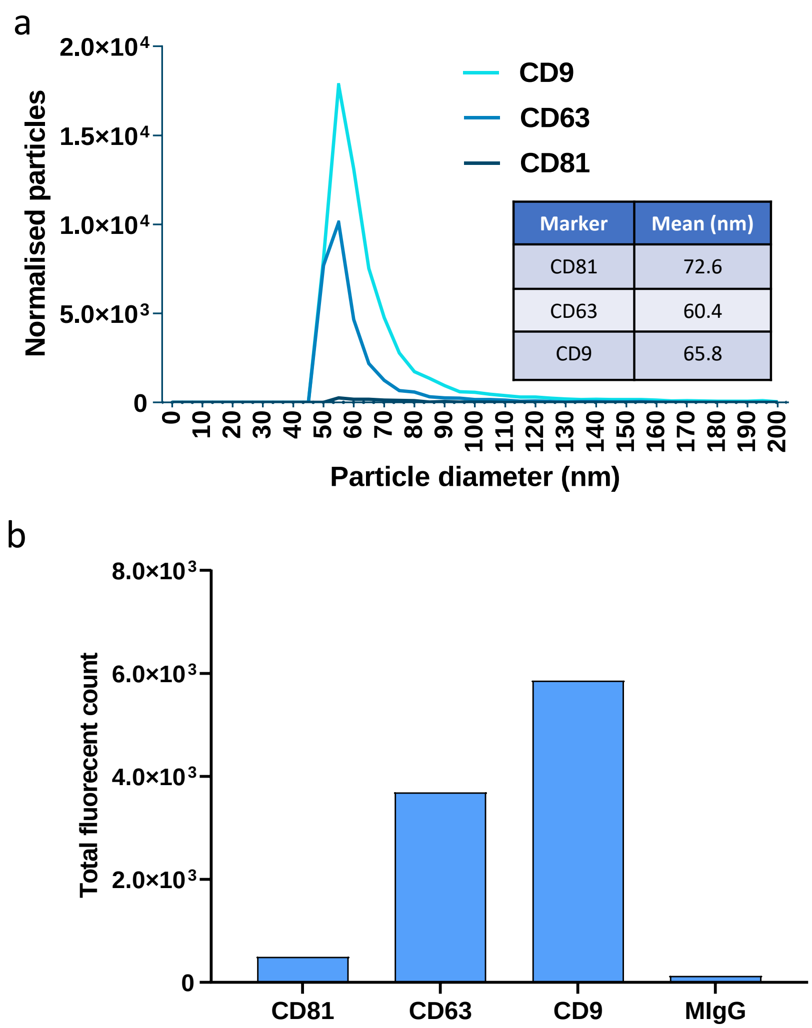

Figure S5. Characterization of the exosomes used in this study. (a) particle size. Sizing is obtained by interferometry-based label free measurements performed on each spot using the ExoView™ R100 system from NanoView Biosciences. The mean is calculated from three spots for each capture antibody, CD81, CD9, and CD63, respectively. Results show the size of the exosomes used were around 45-80 nm. (b) Surface marker expression. Total fluorescent count is quantified based on the number of particles in a defined area of the antibody capture spot (normalised particles). In this example, the total number of fluorescently labelled particles for each spot has been calculated, showing the relative abundance of each tetraspanin, CD9, CD63, and CD81.

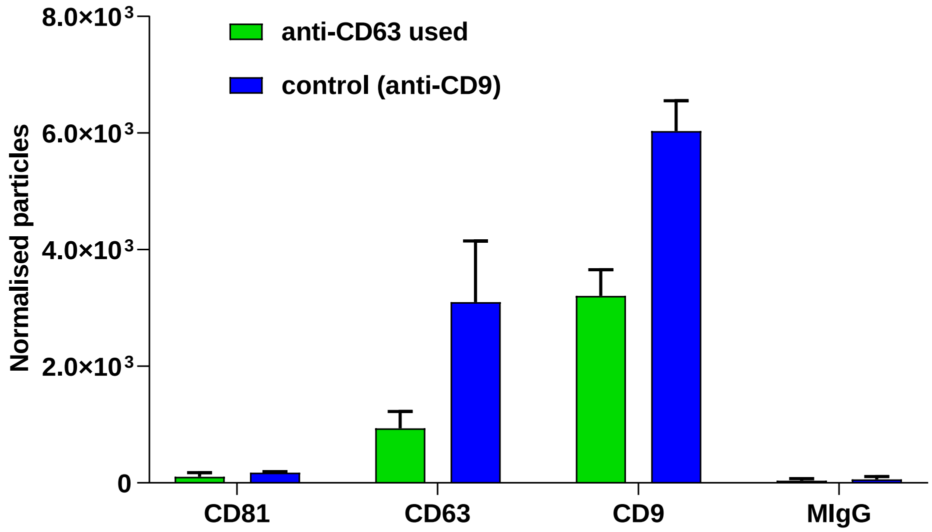

Figure S6. Validation of the binding ability of the anti-CD63 used in this study. Labelling bound vesicles with fluorescently conjugated antibodies allows for detailed analysis of vesicle subpopulations. Fluorescent labelling of captured vesicles was performed using the anti-human CD63 conjugated to Alexa568 (which is used in the study for binding to exosomes). To avoid competition, the standard CD63 Ab was not included in the fluorescent cocktail. Similarly, CD81 was not included since Alexa568 is detected in the green channel. Only CD9 antibody is included as a control (reference) for interpreting the binding abundance of the tested anti-CD63. Results demonstrate good binding and specificity of anti-human CD63 for captured vesicles.

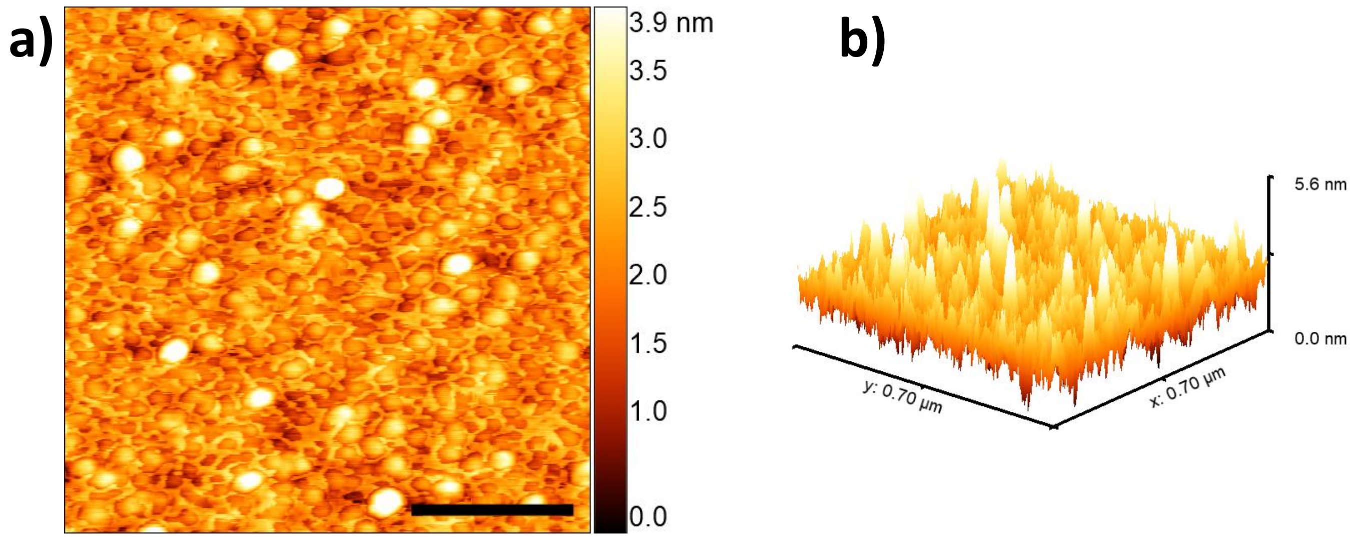

Figure S7. AFM profile of CD63 on the graphene surface. a) 2D profile showing the distribution of Ab on the graphene surface. b) 3D AFM profile of the same spot. Scale bar =200nm.

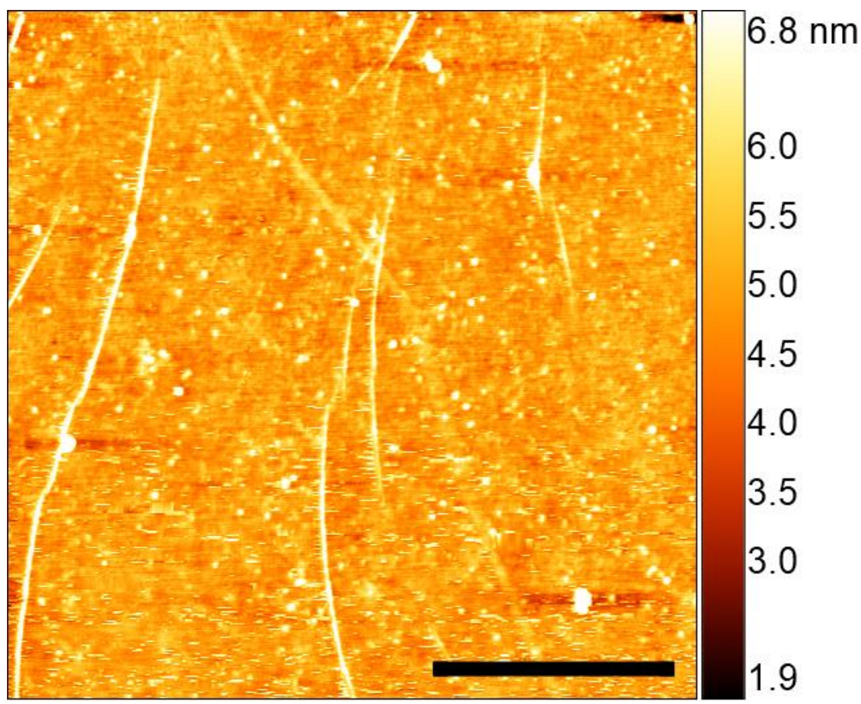

Figure S8. AFM profile of IgG1κ isotype on graphene surface (rms=0.63 nm); Scale bar =1µm.

Section3. Dirac voltage stability, hysteresis and ionic strength measurements

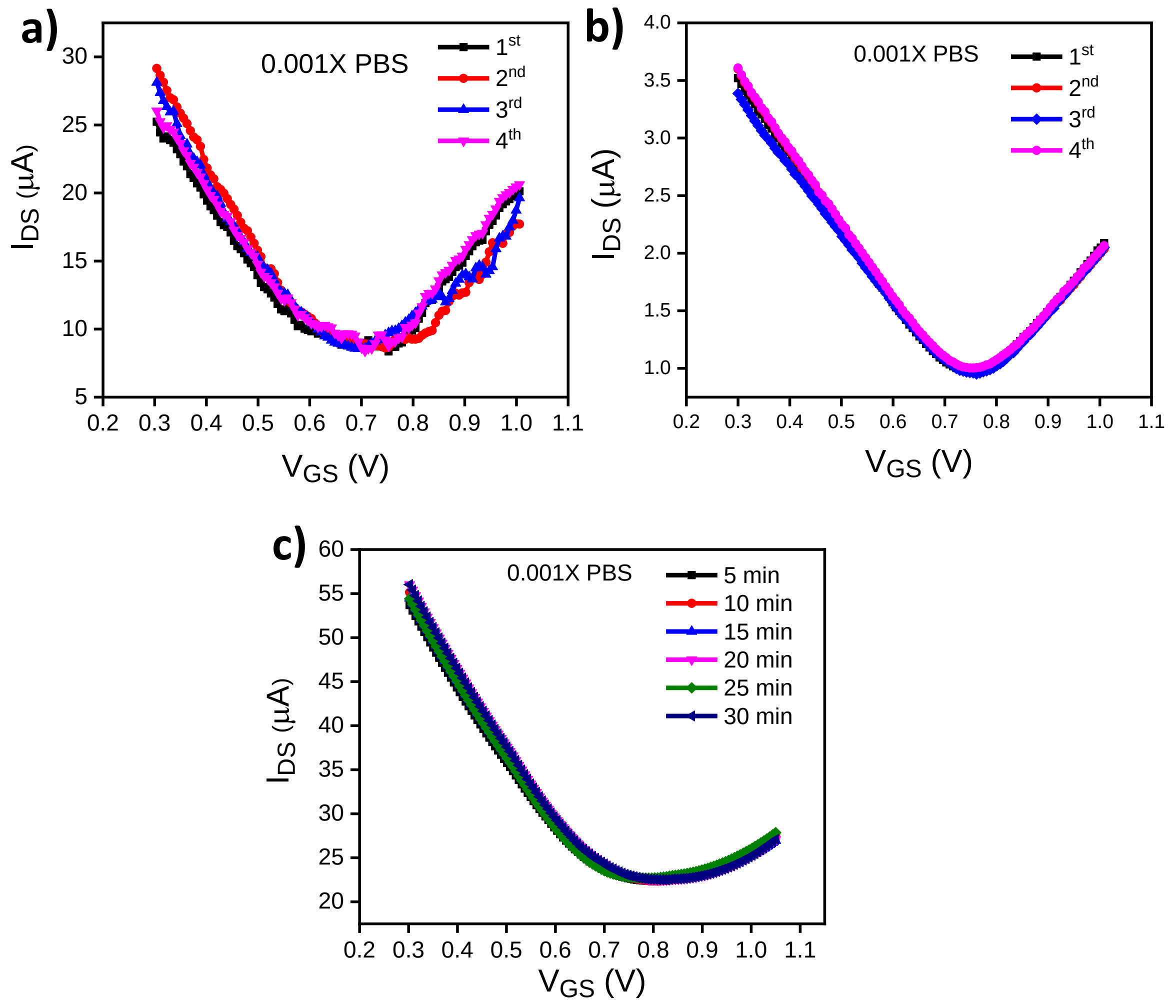

Figure S9. Stability of different devices in buffer solution. (a) and (b) after different rinsing with PBS; (c) change in Dirac voltage over time in 0.001X PBS.

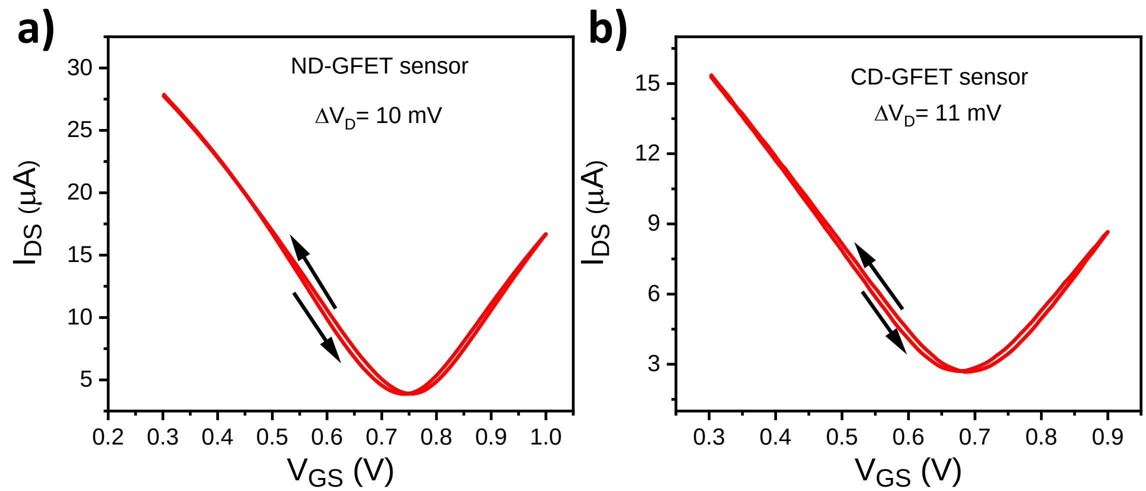

Figure S10. Transfer characteristics (IDS vs VGS) under forward and backward gate voltage sweep for (a) ND-GFET and (b) CD-GFET sensors.

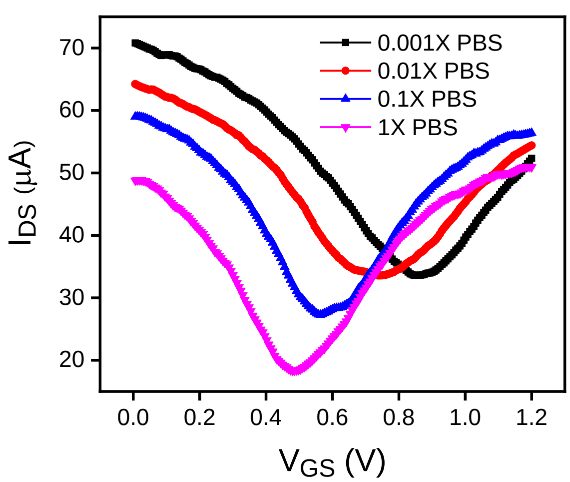

Figure S11. Transfer characteristics (I_{DS} vs V_{GS}) of GFETs in different ionic strength 0.001X PBS, 0.01X PBS, 0.1 PBS, 1X PBS.

Section S4. Electrical tests of exosome on ND-GFET and CD-GFET sensors

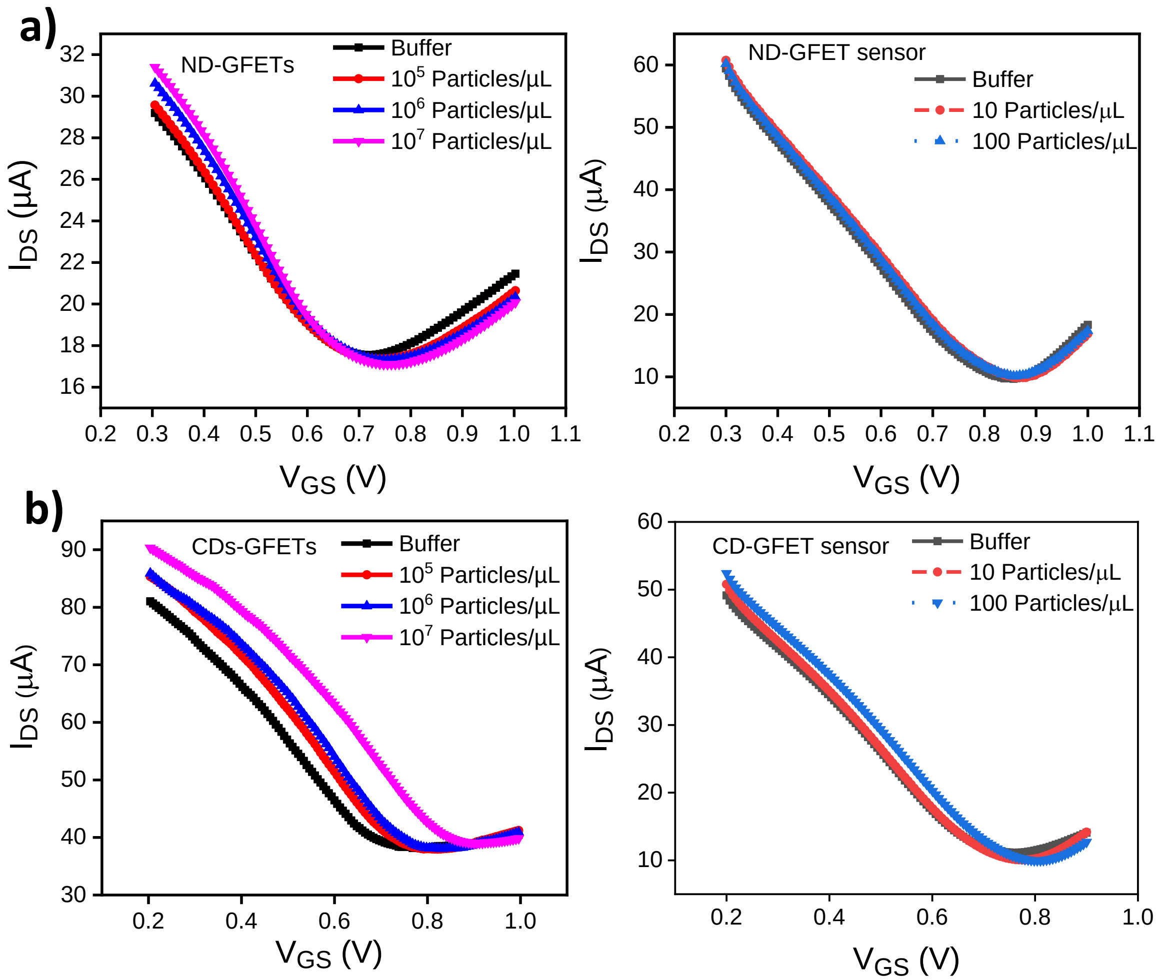

Figure S12. I_{DS}-V_{GS} of (a) non-decorated FETs and (b) CD-FETs with different concentration of exosome.

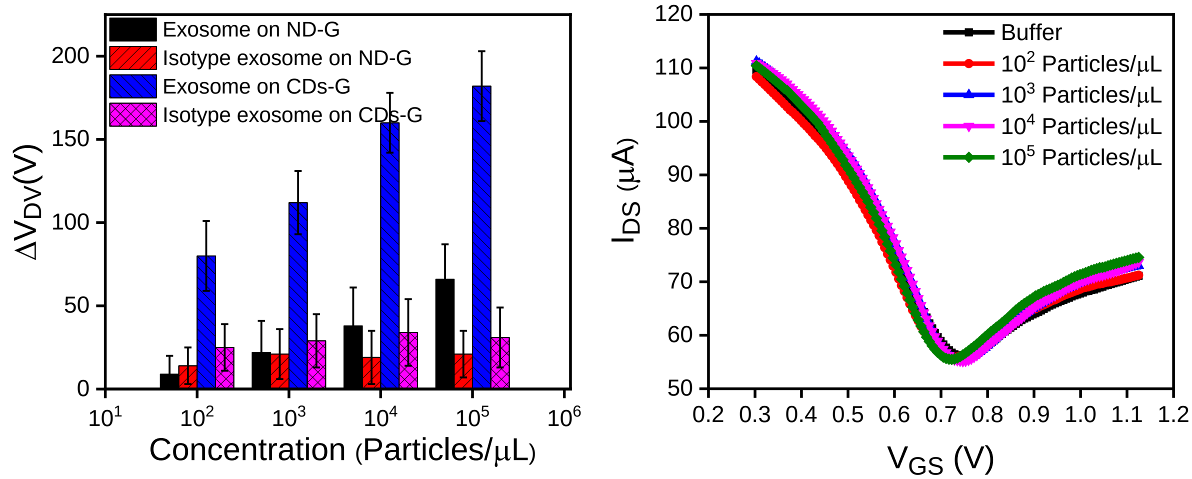

Figure S13. (a) Dirac voltage shift of ND-GFETs and CDs-GFETs sensors for exosome and isotype conjugated control sample; (b) I_{DS}-V_{GS} for CD-FETs with different concentration of exosome for isotype conjugated samples.

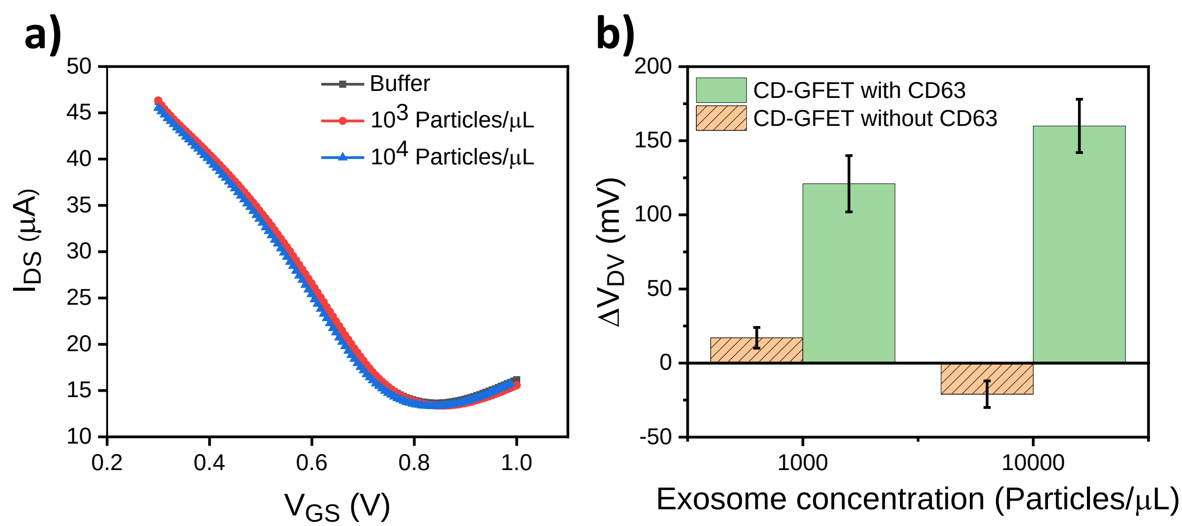

Figure S14. Measured I_{DS}-V_{GS} for CD-FETs for different concentrations of exosome for CD-GFET sensors without CD63 functionalization (n=5). (b) Dirac voltage shift of CDs-GFET sensors for exosome with and without CD63 functionalization.

- **Fitting the shift in Dirac voltage as a function of exosome concentration**

The Sips model is used to fit the shift in Dirac voltage as a function of exosome concentration in Figure 4d. This model has been previously used for describing the DNA hybridization to fit the Dirac voltage change in GFET sensor with target concentration.[1, 2] However, Sips hasn't been used before to fit the binding kinetics of exosome. The general equation that describes the Sip model is given by:

$$\Delta V_{DV} = V_{Max} \frac{(\frac{C}{K_D})^a}{1 + (\frac{C}{K_D})^a} \qquad S1$$

Table S2. Fitting parameters of Dirac voltage as a function of exosome concentration based on Sips model

Fitting parameter	ND-GFET sensor	CD-GFET sensor
V_{DMAX} (mV)	120	208
K_D(Exosome/mL)	10^8	10^6
a	0.2	0.35

The value of K_D is 100 times lower than the reported in literature.[3] It is possible that the measurements in low buffer concentration[4] has enhanced the affinity of antibodies with the exosomes. However, the role of CDs in enhancing the CD63-exosome interaction is not clear.

- **Time measurements fitting**

$$\Delta V_D = \Delta V_{DMAX}(1 - e^{-\tau t}) \qquad S2$$

Table S3. Fitting parameters of change in Dirac voltage as a function of time

Fitting parameter	ND-GFET sensor	CD-GFET sensor
ΔV_{DMAX} (mV)	85.70	187.15
$\tau(1/Sec)$	0.07	0.19

Table S3 shows that the response of the CDs-GFET sensors is twice as fast as ND-FET sensors.

Section S5. Calculation of exosome accumulation time for nanosphere and flat surface in pure diffusion regime

The number of molecules accumulated on the sensor at a given time can be written as[5]:

$$\mathrm{N(t)} = N_A C_o t(\frac{A_D}{C_D(t)} + \frac{1}{K_{on} b_m})^{-1} \qquad S3$$

where NA is the Avogadro's number, C_0 is the initial analyte concentration, CD(t) is the diffusion capacitance and can be calculated by using an analogy to the electrostatic capacitance. CD(t) is given by[5]:

$$C_D(t) = \begin{cases} \dfrac{D}{\sqrt{2Dt}} & Flat \\ \dfrac{4\pi D}{a^{-1} - (\sqrt{6Dt} + a)^{-1}} & Sphere \end{cases} \qquad S4$$

where D is the diffusion coefficient and a is the nanosphere radius.

$$D = \frac{K_B T}{6\pi\eta r} \qquad S5$$

η viscosity; r radius of the molecules; T temperature and KB is Boltzmann constant. The value of D for exosome is extracted from Figure S9. The accumulation of molecules at the sensor surface proportional with (t) for spherical sensor and ($\sqrt{t}$) for planar sensor.

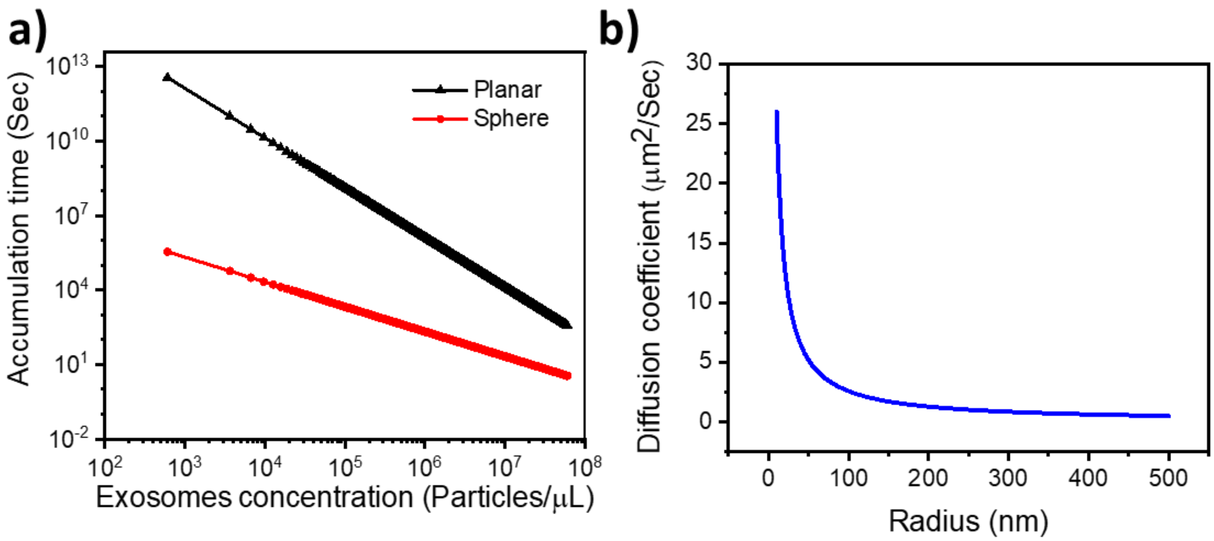

Figure S15. (a) Calculated accumulation time required to capture exosomes on spherical and flat surface (a=10 nm; N=2 μm^{-2}). (b) calculation of diffusion coefficient as a function of particle radius.

Section S6. Electrical measurements of CDs under dry conditions

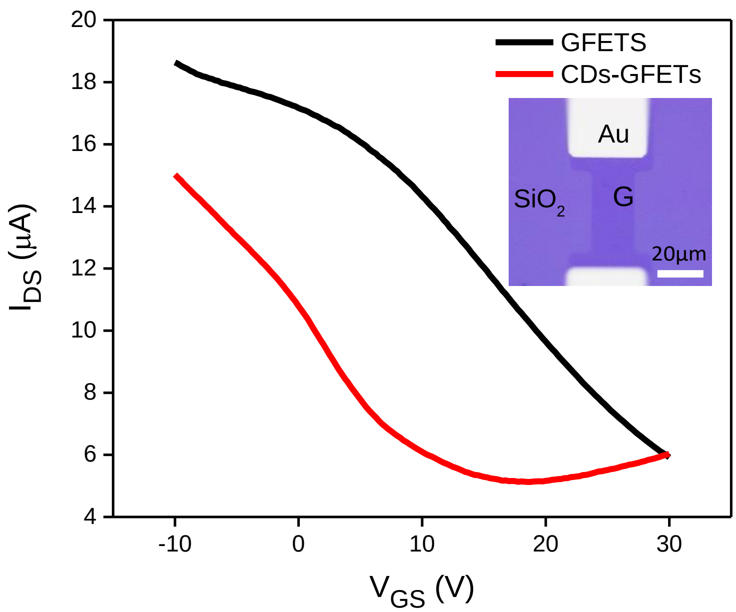

Figure S16. I_{DS}-V_{GS} showing the effect of CDs on electrical properties of FETs.

References:

1. Ping, J.; Vishnubhotla, R.; Vrudhula, A.; Johnson, A. T. C., Scalable Production of High-Sensitivity, Label-Free DNA Biosensors Based on Back-Gated Graphene Field Effect Transistors. *ACS Nano* **2016,** *10* (9), 8700-8704.
2. Hwang, M. T.; Heiranian, M.; Kim, Y.; You, S.; Leem, J.; Taqieddin, A.; Faramarzi, V.; Jing, Y.; Park, I.; van der Zande, A. M.; Nam, S.; Aluru, N. R.; Bashir, R., Ultrasensitive detection of nucleic acids using deformed graphene channel field effect biosensors. *Nature Communications* **2020,** *11* (1), 1543.
3. Wang, Y.; Yuan, W.; Kimber, M.; Lu, M.; Dong, L., Rapid Differentiation of Host and Parasitic Exosome Vesicles Using Microfluidic Photonic Crystal Biosensor. *ACS Sensors* **2018,** *3* (9), 1616-1621.
4. Wallis, R.; Moore, G. R.; James, R.; Kleanthous, C., Protein-Protein Interactions in Colicin E9 DNase-Immunity Protein Complexes. 1. Diffusion-Controlled Association and Femtomolar Binding for the Cognate Complex. *Biochemistry* **1995,** *34* (42), 13743-13750.
5. Nair, P. R.; Alam, M. A., Performance limits of nanobiosensors. *Applied Physics Letters* **2006,** *88* (23), 233120.